引用格式：YANG Yuqiang, ZHANG Yuying, LI Yuting, et al. Fiber Optic Temperature Sensor Based on Harmonic Vernier Effect of Sagnac Interferometer[J]. Acta Photonica Sinica, 2024, 53(4):0406004
杨玉强,张钰颖,李雨婷,等.基于Sagnac干涉计谐波游标效应的光纤温度传感器[J].光子学报,2024,53(4):0406004

基于Sagnac干涉计谐波游标效应的光纤温度传感器

杨玉强[1,2,3],张钰颖[2,3],李雨婷[2,3],高佳乐[2,3],牟小光[4],毕磊[5]

(1 广东海洋大学 深圳研究院,深圳 518120)
(2 广东海洋大学 广东省南海海洋牧场智能装备重点实验室,湛江 524088)
(3 广东海洋大学 智慧海洋传感网及其装备工程技术研究中心,湛江 524088)
(4 广东海洋大学 机械工程学院,湛江 524088)
(5 广东海洋大学 继续教育学院,湛江 524088)

摘 要:提出一种基于双萨格奈克(Sagnac)干涉计谐波游标效应的光纤温度传感器,在该传感器中,传感干涉计中熊猫光纤的长度约为参考干涉计中熊猫光纤的整数倍。理论分析与实验结果表明,当游标放大倍率相同时,基于谐波游标效应和基于普通光学游标效应的双Sagnac干涉计具有相同的温度灵敏度,但谐波游标效应对应的熊猫光纤长度失谐量明显大于普通光学游标效应,且阶数越高对应的失谐量越大。由于失谐量越大,游标放大倍率越容易控制和实现,因此,从制备角度上讲,谐波游标效应明显优于普通光学游标效应。该研究可为后续光学游标效应的研究提供重要参考。

关键词:光纤传感器;Sagnac干涉计;谐波游标效应;普通游标效应;温度传感
中图分类号:O436 **文献标识码**:A **doi**:10.3788/gzxb20245304.0406004

0 引言

光纤干涉计在光学检测中起着非常重要的作用,由于其体积小、重量轻、抗腐蚀、抗电磁干扰、灵敏度高等优点,被广泛应用于温度、湿度、磁场、应变等参数的测量[1-4]。光纤干涉计主要分为法布里-珀罗干涉计(Fabry-Perot Interferometer,FPI)、马赫-曾德干涉计、迈克尔逊干涉计和Sagnac干涉计(Sagnac Interferometer,SI)等[5-6],尽管单个光纤干涉计的灵敏度可以达到nm/℃量级,但仍然不能满足某些应用领域的特殊需求。

近年来,研究人员将两个光纤干涉计级联或并联,使其产生光学游标效应,大幅提高了干涉型光纤传感器的测量灵敏度[7-10]。当两光纤干涉计的自由光谱范围接近但不相等时,产生的游标效应称为普通光学游标效应[11-12],当一个光纤干涉计的自由光谱范围约为另一个光纤干涉计的整数倍时,产生的游标效应称为谐波游标效应。2014年,ZHANG Peng等[13]将两个自由光谱范围相近的FPI干涉计级联,实现了普通光学游标效应。2015年,SHAO Liyang等[14]将两个自由光谱范围接近的SI干涉计级联实现了高灵敏度温度传感,级联后传感器的温度灵敏度约为单个SI的9倍。2019年,GOMES A D等[15]提出了谐波游标效应,并于2020年[16]成功制备出基于1阶谐波游标效应的双FPI传感器,该传感器的温度和应变灵敏度分别为−650 pm/℃和146.3 pm/με。2021年,LIU Shuang等[17]研究了两个SI干涉计级联1阶和2阶谐波游标效应,

基金项目:广东省自然科学基金面上项目(Nos. 2023A1515011212, 2022A1515011603),深圳市基础研究面上项目(Nos. JCYJ20210324122813036, JCYJ20220530162200001),广东省普通高校重点领域专项(No. 2021ZDZX1015),广东海洋大学科研启动经费资助项目(No. 060302112009)
第一作者:杨玉强,yuqiangy110@sina.com
通讯作者:牟小光,mouxg@gdou.edu.cn
收稿日期:2023-09-12;**录用日期**:2023-10-23

研究了其温度传感特性。相比普通光学游标效应，谐波游标效应中两个光纤干涉计的自由光谱范围约为整数倍关系，不受1倍关系的限制，因此，谐波游标效应比普通光学游标效应的设计自由度更大，制备难度更低。然而，以上研究均未就谐波游标效应的以上优点进行深入分析。

本文提出并制备了一种基于谐波游标效应的双SI温度传感器，在该传感器中，参考SI的自由光谱范围约为传感SI的整数倍。对比分析了产生0阶、1阶和2阶谐波游标效应且放大倍率相同时传感器的温度灵敏度及熊猫光纤长度失谐量，并进行了实验验证，结果表明：当游标放大倍率相同时，基于不同谐波游标效应的光纤传感器的温度灵敏度几乎相同，但不同谐波游标效应对应的熊猫光纤失谐量明显不同，且谐波阶次越高，失谐量越大。

1 传感器原理与仿真分析

本文提出的传感器结构如图1，干涉计SI1和SI2为并联结构，分别连接在光纤耦合器（Coupler，C）C3的两个输出端上，其中，SI1为参考干涉计，而SI2为传感干涉计，且SI2中熊猫光纤的长度约为SI1中熊猫光纤长度的整数倍。宽谱光源（Broad Band Optical Source，BBS）发生的信号光经SI1和SI2后，由光谱分析仪（Optical Spectrum Analyzer，OSA）接收，光谱分析仪接收到的信号光为干涉计SI1和SI2的叠加。

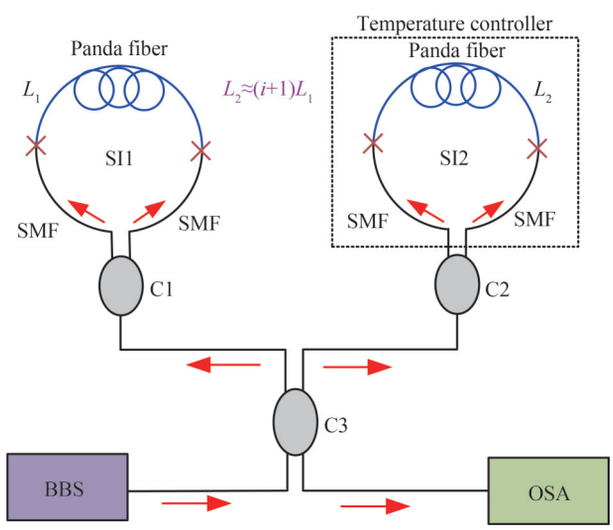

图1 传感器原理

Fig. 1 Schematic of the sensor

Sagnac干涉计SI1和SI2的干涉谱可分别表示为[18]

$$\begin{cases} I_1(\lambda)=\dfrac{I_{01}}{2}\left[1-\cos\left(\dfrac{2\pi BL_1}{\lambda}\right)\right] \\ I_2(\lambda)=\dfrac{I_{02}}{2}\left[1-\cos\left(\dfrac{2\pi BL_2}{\lambda}\right)\right] \end{cases} \tag{1}$$

式中，B为熊猫光纤的双折射系数，L_1和L_2为干涉计SI1和SI2中熊猫光纤的长度。由式(1)推导可知，干涉计SI1和SI2的自由光谱范围分别为

$$\begin{cases} \mathrm{FSR}_1=\dfrac{\lambda_n^2}{BL_1} \\ \mathrm{FSR}_2=\dfrac{\lambda_n^2}{BL_2} \end{cases} \tag{2}$$

式中，λ_n为干涉计第n个谐振峰的波长。式(2)表明，随着熊猫光纤长度的增加，其自由光谱范围也会逐渐减小[19]，由式(1)可知，传感干涉计SI2的温度灵敏度可表示为

$$S_{\mathrm{SI2}}=\frac{\mathrm{d}\lambda_n}{\mathrm{d}T}=\frac{\lambda_n}{B}\frac{\mathrm{d}B}{\mathrm{d}T}+\frac{\lambda_n}{L_2}\frac{\mathrm{d}L_2}{\mathrm{d}T}\approx\frac{\lambda_n}{B}\frac{\mathrm{d}B}{\mathrm{d}T} \tag{3}$$

式(3)表明干涉计SI2的温度灵敏度与双折射系数的温度变化率成正比。由于熊猫光纤的双折射系数随温度的增大而减小，因此，$S<0$，即随着温度的升高，SI的干涉谱向短波方向移动。

光谱分析仪接收到的干涉谱为干涉计SI1和SI2干涉谱的叠加，可表示为

$$I(\lambda)=I_1(\lambda)+I_2(\lambda) \tag{4}$$

当SI2干涉计中熊猫光纤的长度约为SI1干涉计中熊猫光纤长度的$i+1$($i=1,2,3,\cdots$)倍时，两干涉计将产生i阶谐波游标效应[20]，值得提出的是，当$i=0$时，两干涉计产生普通光学游标效应，为便于分析，在后续的讨论中称为0阶谐波游标效应。当产生i阶游标效应时，干涉谱中将出现如图2～4所示的干涉谱包络。当$i=0$时，产生0阶谐波游标效应(普通光学游标效应)，此时干涉谱中将出现如图2所示的单包络；当$i=1$时，产生1阶谐波游标效应，此时干涉谱中将出现如图3所示的双包络(双包络为每间隔1个点取1点构成的波谷曲线)；当$i=2$时，产生2阶游标效应，此时干涉谱中将出现如图4所示的三包络(三包络为每间隔2个点取1点构成的波谷曲线)；其他情况，依次类推。

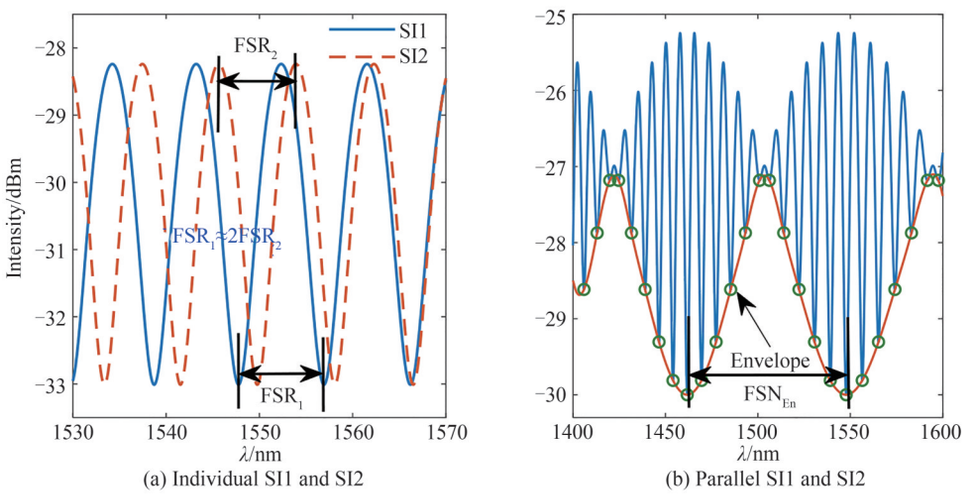

图2　普通光学游标效应对应的干涉谱

Fig. 2　Interference spectra of normal Vernier effect

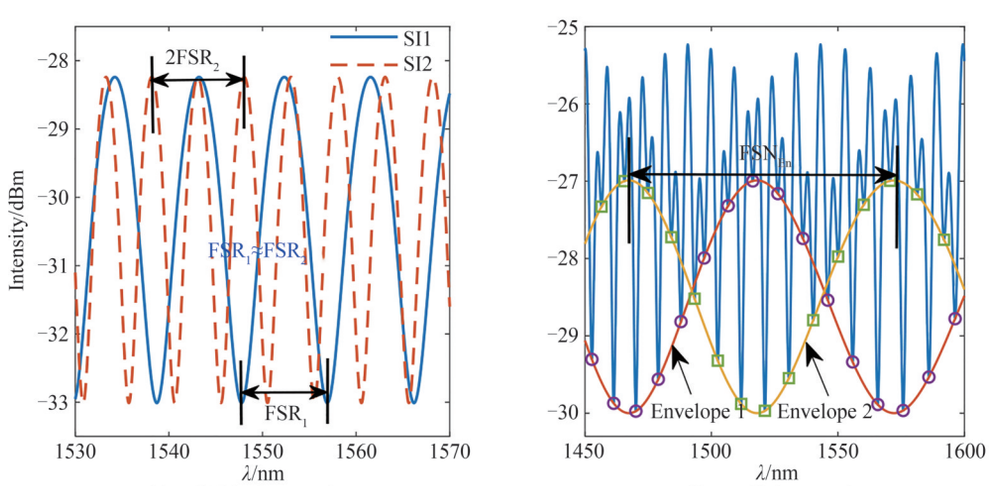

图3　1阶谐波游标效应对应的干涉谱

Fig. 3　Interference spectra of first-order harmonic Vernier effect

当干涉计SI1和SI2产生i阶谐波游标效应时，干涉谱内包络的自由光谱范围可表示为

$$\mathrm{FSR_{En}}^{i}=\frac{\mathrm{FSR_1}\cdot(i+1)\,\mathrm{FSR_2}^{i}}{|\mathrm{FSR_1}-(i+1)\,\mathrm{FSR_2}^{i}|} \tag{5}$$

式中，$\mathrm{FSR_2}^{i}$为产生i阶游标效应时，干涉计SI2的自由光谱范围。i阶谐波游标效应的放大倍率M^i可表示为

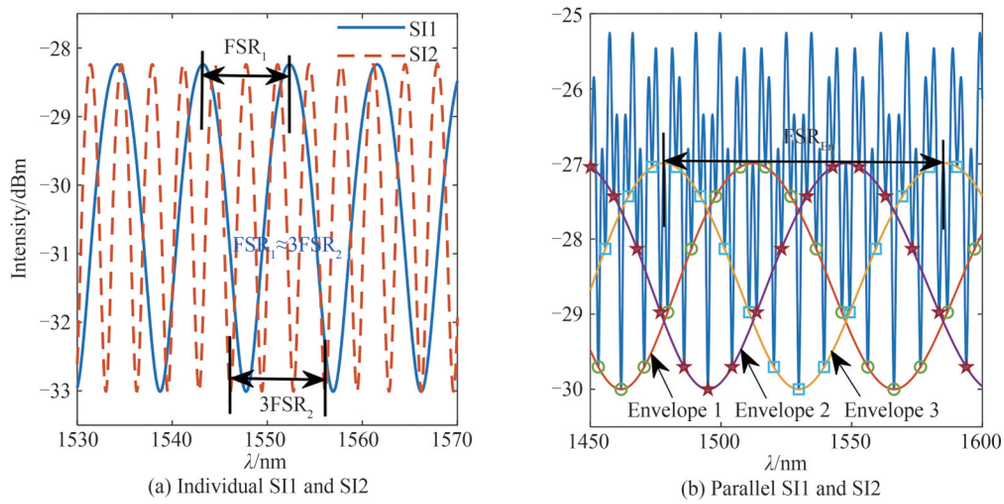

图4 2阶谐波游标效应对应的干涉谱

Fig. 4 Interference spectra of second-order harmonic Vernier effect

$$M^i=\frac{\mathrm{FSR}_1}{|\mathrm{FSR}_1-(i+1)\mathrm{FSR}_2^i|}=\frac{\mathrm{FSR}_1}{|\Delta\mathrm{FSR}^i|} \tag{6}$$

式中，$\Delta\mathrm{FSR}^i=(i+1)\ \mathrm{FSR}_2{}^i-\mathrm{FSR}_1$为产生$i$阶谐波游标效应时，干涉计SI2的自由光谱范围失谐量。

将式(2)代入式(6)得

$$M^i=\frac{L_2^i}{|L_2^i-(i+1)L_1|}=\frac{L_2^i}{|\Delta L_2^i|} \tag{7}$$

式中，$\Delta L_2^i=L_2^i-(\mathrm{i}+1)\ L_1$为产生$i$阶谐波光学游标效应时干涉计SI2中熊猫光纤的长度失谐量。当谐波游标效应和普通光学游标效应的放大倍率相同时，即$M^i=M^0$，同时考虑到$L_2^0\approx L_1$，$L_2^i\approx(i+1)L_1$，则

$$\left|\Delta L_2^i\right|\approx(i+1)\left|\Delta L_2^0\right| \tag{8}$$

式中，ΔL_2^0和ΔL_2^i分别为普通光学游标效应和谐波游标效应熊猫光纤失谐量。由式(8)可知，当游标放大倍率相同时，产生i阶谐波游标效应所需的熊猫光纤失谐量为产生普通光学游标效应的$i+1$倍。从传感器制备角度讲，熊猫光纤失谐量越大越容易控制，制备难度越小。

由于在该传感器中，SI1为参考干涉计，而SI2为传感干涉计，因此，该传感器的灵敏度可表示为

$$S_{\mathrm{En}}{}^i=\begin{cases}M^iS_{\mathrm{SI2}} & (\mathrm{FSR}_1>(i+1)\mathrm{FSR}_2^i)\\ -M^iS_{\mathrm{SI2}} & (\mathrm{FSR}_1<(i+1)\mathrm{FSR}_2^i)\end{cases} \tag{9}$$

式(9)表明，当$\mathrm{FSR}_1>(i+1)\mathrm{FSR}_2{}^i$时，干涉谱包络与干涉计SI2干涉谱具有相同的移动方向；当$\mathrm{FSR}_1<(i+1)\ \mathrm{FSR}_2{}^i$时，干涉谱包络与干涉计SI2干涉谱具有相反的移动方向。

对以上分析进行数值仿真，仿真参数为：$I_{01}=I_{02}=0.02$，$B=5.06\times10^{-4}$，$\mathrm{d}B/\mathrm{d}T=-6.1\times10^{-7}$，$L_1=520$ mm，$L_2^0=572$ mm、$L_2^1=953$ mm、$L_2^2=1\ 430$ mm。图5(a)为恒温下干涉计SI1的干涉谱，可知SI1的自由光谱范围为9.13 nm。当温度分别为T_0 ℃和T_0+1 ℃时，干涉计SI2的干涉谱如图5(b)、5(c)和5(d)，可知，当熊猫光纤的长度分别为$L_2^0=572$ mm、$L_2^1=953$ mm、$L_2^2=1\ 430$ mm时，SI2干涉计的自由光谱范围分别为$\mathrm{FSR}_2^0=8.30$ nm、$\mathrm{FSR}_2^1=4.98$ nm和$\mathrm{FSR}_2^2=3.32$ nm。当温度由T_0 ℃升高到T_0+1 ℃时，不同熊猫光纤长度的SI2干涉计的干涉谱均向短波方向移动，移动量均约为1.89 nm，表明干涉计SI2的温度灵敏度与熊猫光纤的长度无关，该结果与式(3)分析结果相吻合。

当温度分别为T_0 ℃和T_0+1 ℃时，干涉计SI1与SI2的并联干涉谱如图6。由图6可知，当干涉计SI2中熊猫光纤长度为$L_2^0=572$ mm、$L_2^1=953$ mm和$L_2^2=1\ 430$ mm时，与干涉计SI1的并联干涉谱中分别出现了单包络、双包络和三包络，表明两干涉计分别产生了0阶、1阶和2阶谐波游标效应，由式(6)计算可知0阶、1阶和2阶谐波游标效应的放大倍率均为11倍。当温度由T_0 ℃升高到T_0+1 ℃时，单包络向短波方向移动，而双包络和三包络均向长波方向移动，与单个SI2的移动方向相反。原因在于，对于单包络，两干涉计的自由光

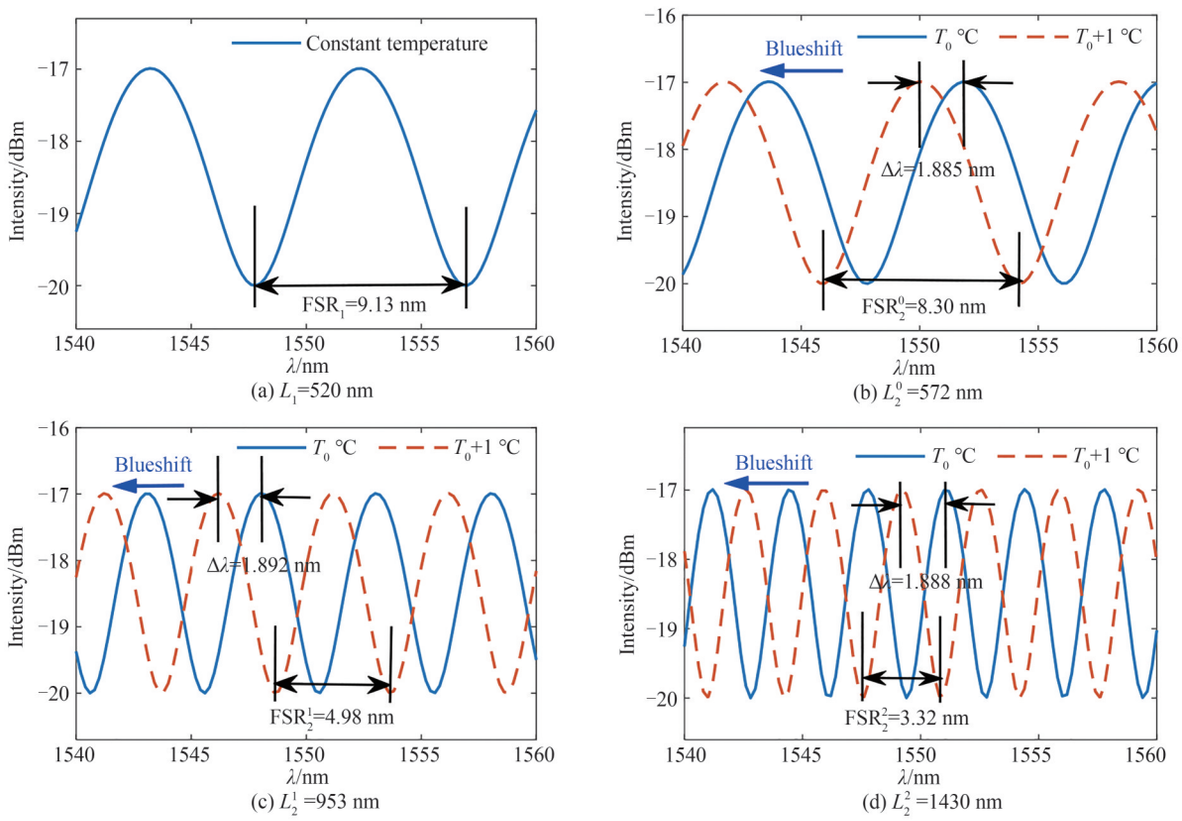

图5　SI1和SI2的干涉谱

Fig. 5　Interference spectra of individual SI1 and SI2

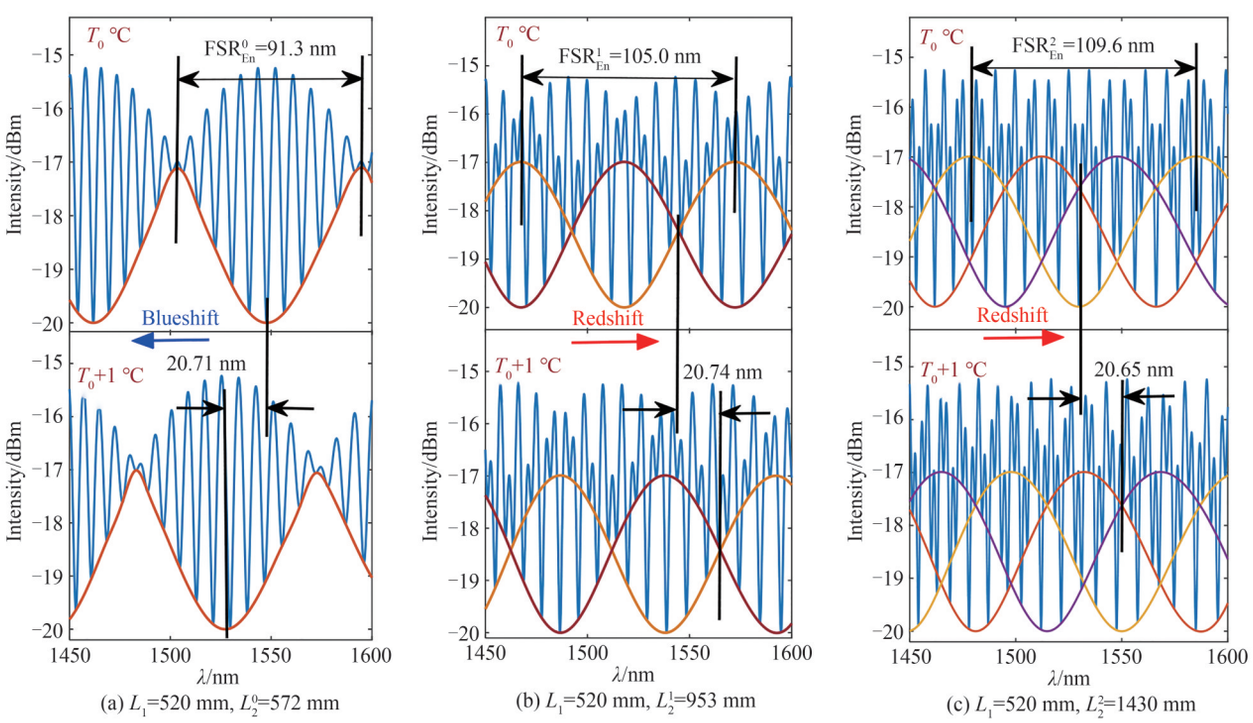

图6　温度分别为T_0 ℃和T_0+1 ℃时，干涉计SI1和SI2的并联干涉谱

Fig. 6　Parallel interference spectra of SI1 and SI2 at temperatures T_0 ℃ and T_0+1 ℃

谱范围满足$FSR_2^0<FSR_1$，由式(9)可知，此情况下单包络的移动方向与单个SI2的移动方向相同；对于双包络和三包络，两干涉计的自由光谱范围分别满足$2FSR_2^1>FSR_1$和$3FSR_2^2>FSR_1$，由式(9)可知，此情况下双

包络和三包络的移动方向与单个SI2的移动方向相反。此外，单包络、双包络和三包络的移动量均约为20.7 nm，原因在于，0阶、1阶和2阶游标效应的游标放大倍率相同。

2 实验与分析

传感器实验装置如图1，包括宽谱光源（型号为Golight，波长范围为1 400～1 600 nm），光纤耦合器C1、C2和C3，光谱分析仪（型号为Ceyear 6362D，分辨率为0.02 nm），干涉计SI1和SI2。宽谱光源发出的信号光经SI1和SI2后由光谱分析仪接收。干涉计SI1和SI2均由单模光纤环内熔接一段熊猫光纤构成，传感器中，SI1为参考干涉计，其温度保持不变，而SI2为传感干涉计，置于温控箱内，与温控箱的温度保持一致，温控箱的温度精度为0.1 ℃。SI1中熊猫光纤的长度L_1=520 mm，而SI2中熊猫光纤的长度分别为L_2^0=572 mm、L_2^1=953 mm和L_2^2=1 430 mm。

图7(a)为恒温下SI1的干涉谱，可知，SI干涉计的自由光谱范围为FSR_1=9.13 nm。图7(b)、7(c)和7(d)分别为40 ℃和41 ℃时不同熊猫光纤长度SI2的干涉谱，可知，熊猫光纤长度分别为L_2^0=572 mm、L_2^1=953 mm和L_2^2=1 430 mm的干涉计SI2的自由光谱范围分别为FSR_2^0=8.30 nm、FSR_2^1=4.98 nm和FSR_2^2=3.32 nm。由此可知，$FSR_1 > FSR_2^0$、$FSR_1 < 2\,FSR_2^1$和$FSR_1 < 3\,FSR_2^2$（参考SI干涉计的自由光谱范围FSR_1=9.13 nm）。当温度由40 ℃增加到41 ℃时，SI2的干涉谱均蓝移，移动量均约为1.89 nm。以上实验结果表明，SI2干涉计的温度敏感与熊猫光纤长度无关。

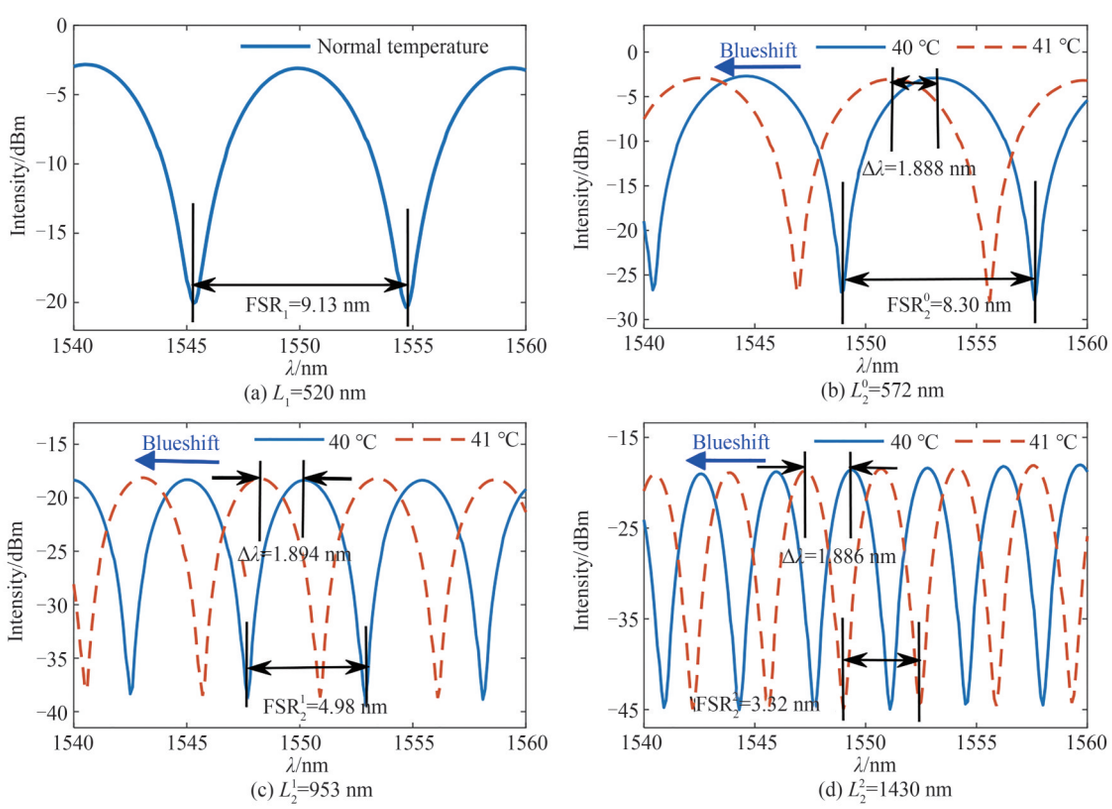

图7 SI1和SI2的干涉谱

Fig. 7 Interference spectra of individual SI1 and SI2

图8为不同温度下，SI1与SI2的并联干涉谱，可知，当SI2中熊猫光纤长度为L_2^0=572 mm、L_2^1=953 mm和L_2^2=1 430 mm时，SI1和SI2并联干涉谱中分别出现了单包络、双包络和三包络，表明两干涉计分别产生了0阶、1阶和2阶谐波游标效应。当温度由40 ℃升高到41 ℃时，单包络向短波方向移动，而双包络和三包络均向长波方向移动，与单个SI2的移动方向相反，移动量均约为20.7 nm。以上实验结果与仿真结果一致。

图9(a)为不同熊猫光纤长度SI2的干涉谱峰值随温度的变化曲线，可知，在40 ℃～50 ℃的温度变化范围内，当熊猫光纤长度分别为L_2^0=572 mm、L_2^1=953 mm和L_2^2=1 430 mm时，SI2干涉计的温度灵敏度分别

为－1.888 nm/℃、－1.894 nm/℃和－1.886 nm/℃，均约为1.89 nm/℃，表明SI2的温度灵敏度与熊猫光纤长度无关，该结果与理论分析结果相吻合。图9(b)为SI1和SI2并联干涉谱包络随温度的变化曲线，可知，在40 ℃～50 ℃的温度变化范围内，单包络、双包络和三包络的温度灵敏度分别为－20.67 nm/℃、21.34 nm/℃和21.18 nm/℃，均约为21 nm/℃，考虑到对应的0次、1次和2次谐波游标效应的放大倍率相同，结果表明当放大倍率相同时，基于谐波游标效应和普通光学游标效应的传感器具有相同的灵敏度，该实验结果与理论分析结果相吻合。

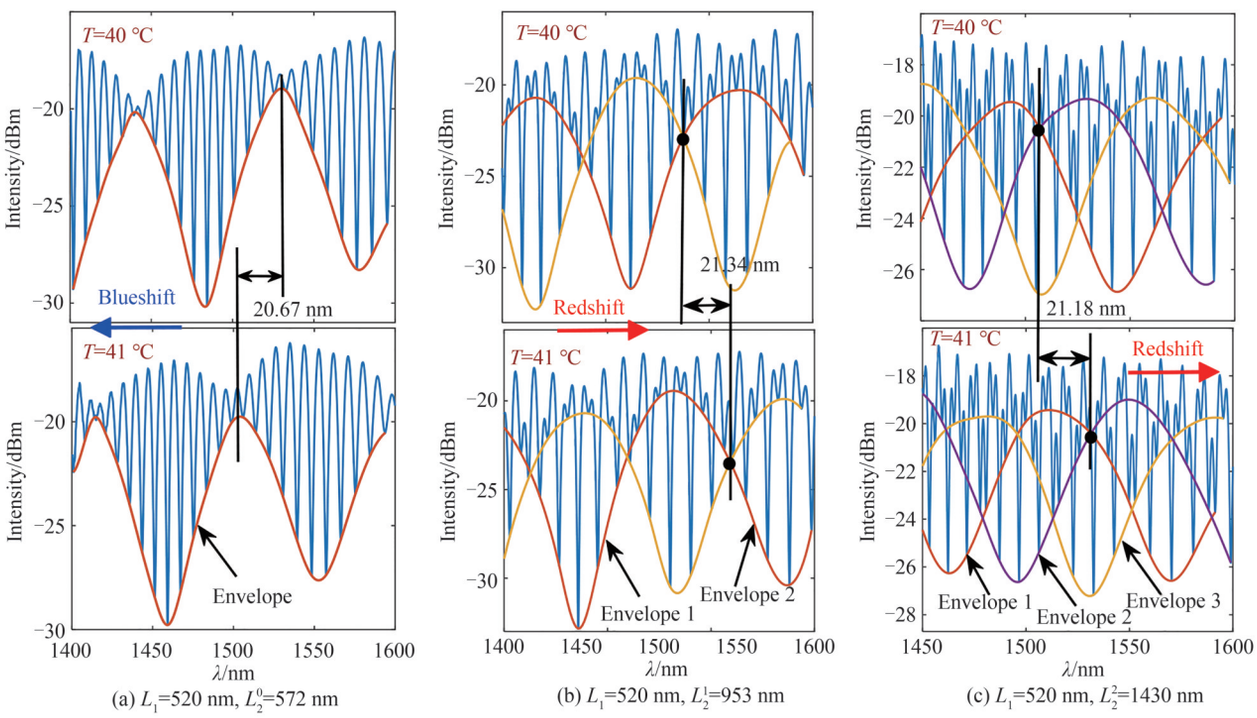

图8　当温度为40 ℃和41 ℃时，SI1和SI2的并联干涉谱

Fig. 8　Parallel interference spectra of SI1 and SI2 at temperatures of 40 ℃ and 41 ℃

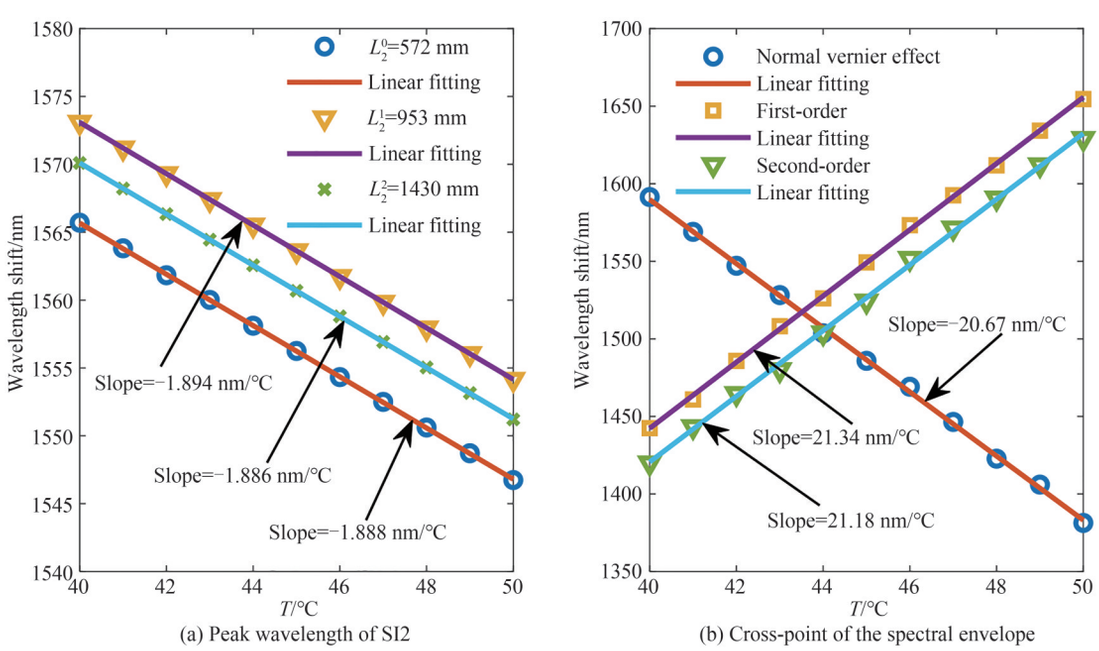

图9　干涉谱峰值波长或交叉点波长随温度的变化曲线

Fig. 9　Peak wavelength /cross-point of the spectrum versus temperature

表1为该传感器产生普通和谐波游标效应时各参量的对比情况。当熊猫光纤长度分别为572 mm、953 mm和1 430 mm的传感干涉计SI2与熊猫光纤长度为520 mm的参考干涉计SI1并联后，分别产生了普通光学游标效应、1阶谐波游标效应和2阶谐波游标效应，且以上游标效应的放大倍率均约为11倍。尽管放大倍率相同，谐波游标效应和普通光学游标效应对应的熊猫光纤长度失谐量明显不同，普通光学游标对应的失谐量为52 mm，而1阶和2阶谐波游标对应的失谐量分别为－87 mm和－130 mm，谐波游标效应对应的失谐量明显大于普通光学游标效应，且阶数越高对应的失谐量越大，该结果与式(8)相吻合。由于失谐量越大，游标放大倍率越容易控制和实现，因此，从制备难度上讲，谐波游标效应明显优于普通光学游标效应。

表1 普通光学游标效应和谐波游标效应对应的各参量对比

Table 1 Comparison of the parameters corresponding to the normal and harmonic Vernier effects

Vernier effect	L_1/mm	L_2^i/mm	S_{SI2}/(nm·℃$^{-1}$)	S_{En}^i/(nm·℃$^{-1}$)	M^i	ΔL_2^i/mm
Normal	520	572	－1.888	－20.67	10.95	52
First-order	520	953	－1.894	21.34	11.27	－87
Second-order	520	1 430	－1.886	21.18	11.23	－130

3 结论

本文提出一种基于双Sagnac干涉计并联的光纤温度传感器，在该传感器中，传感干涉计的熊猫光纤长度约为参考干涉计的整数倍，因此，两干涉计产生了谐波游标效应。以1阶和2阶谐波为例，研究了相同放大倍率条件下，谐波游标效应和普通光学游标效应对应的传感器温度灵敏度及熊猫光纤长度失谐量，实验结果表明，在40 ℃～50 ℃范围内，谐波游标效应和普通光学游标效应对应的光纤传感器具有相同的温度灵敏度，均约为21 nm/℃，约为单个传感干涉计的11倍。然而，谐波游标效应对应的熊猫光纤失谐量明显大于普通光学游标效应，普通光学游标效应对应的失谐量为52 mm，而1阶和2阶谐波游标效应对应的失谐量分别为－87 mm和－130 mm，由此可见，阶数越高失谐量越大，近似呈倍数增加。以上实验结果与理论分析结果相吻合。由于失谐量越大，游标放大倍率越容易控制和实现，因此，从制备角度上讲，谐波游标效应明显优于普通光学游标效应。该研究可为后续光学游标效应的研究提供重要参考。

参考文献

[1] LU Ping, LALAM N, BADAR M, et al. Distributed optical fiber sensing: review and perspective[J]. Applied Physics Reviews, 2019, 6(4): 041302.

[2] APRIYANTO H, RAVET G, BERNAL O D, et al. Comprehensive modeling of multimode fiber sensors for refractive index measurement and experimental validation[J]. Scientific Reports, 2018, 8(1): 5912.

[3] ZHANG Yulan, WU Yongfeng, HAN Yang, et al. High sensitivity strain sensor based on a novel offset-core single micro-tapered fiber-optic Mach-Zehnder interferometer[J]. Optical Fiber Technology, 2022, 73: 103012.

[4] LIN Siyu, ZHANG Yundong, QU Yanchen, et al. A miniature high-temperature fiber-optic sensor based on tip-packaged Fabry-Perot interferometer[J]. Sensors and Actuators A: Physical, 2023, 350: 114122.

[5] ZHAO Chunliu, WANG Zhiqiang, ZHANG Shuqin, et al. Phenomenon in an alcohol not full-filled temperature sensor based on an optical fiber Sagnac interferometer[J]. Optics Letters, 2012, 37(22): 4789-4791.

[6] MANUEL R M, ARRIOJA D A, MIJANGOS J A, et al. Ultra-high-sensitivity temperature sensor using a fiber loop mirror based on a water-filled asymmetric two-hole fiber[J]. IEEE Sensors Journal, 2020, 20(11): 5953-5961.

[7] YANG Yuqiang, WANG Yongguang, ZHAO Yuxin, et al. Sensitivity-enhanced temperature sensor by hybrid cascaded configuration of a Sagnac loop and a F-P cavity[J]. Optics Express, 2017, 25(26): 33290-33296.

[8] ZHOU Xuefang, ZHOU Yu, LI Zengyang, et al. Research on temperature sensing characteristics with cascaded fiber Sagnac interferometer and fiber Fabry-Perot interferometer-based fiber laser[J]. Optical Engineering, 2019, 58(5): 057103.

[9] SHEN Wanmei, JIANG Chao, GUO Xiaoshan, et al. High sensitivity temperature sensors based on Sagnac interferometers cascading[J]. Laser & Infrared, 2022, 52(5): 740-744.
申万梅, 江超, 郭小珊, 等. 萨格纳克干涉计级联的高灵敏度温度传感器[J]. 激光与红外, 2022, 52(5): 740-744.

[10] CHEN Sijie, PAN Pan, XIE Tongtong, et al. Sensitivity enhanced fiber optic temperature sensor based on optical carrier microwave photonic interferometry with harmonic Vernier effect[J]. Optics & Laser Technology, 2023, 160(2): 109029.

[11] LIU Ji, NAN Pengyu, TIAN Qin, et al. Sensitivity enhanced strain sensor based on two-arm Vernier effect[J]. IEEE Photonics Technology Letters, 2021, 33(8): 375-378.

[12] LIAO Hao, LU Ping, FU Xin, et al. Sensitivity amplification of fiber-optic in-line Mach-Zehnder Interferometer sensors with modified Vernier-effect[J]. Optics Express, 2017, 25(22): 26898-26909.
[13] ZHANG Peng, TANG Ming, GAO Feng, et al. Cascaded fiber-optic Fabry-Perot interferometers with Vernier effect for highly sensitive measurement of axial strain and magnetic field[J]. Optics Express, 2014, 22(16): 19581-19588.
[14] SHAO Liyang, LUO Yuan, ZHANG Zhiyong, et al. Temperature sensor with enhanced sensitivity by cascaded fiber optic Sagnac loops[C]. 23rd International Conference on Optical Fibre Sensors, 2014:915728.
[15] GOMES A D, FERREIRA M S, BIERLICH J, et al. Optical harmonic Vernier effect: A new tool for high performance interferometric fiber sensors[J]. Sensors, 2019, 19(24): 5431.
[16] GOMES A D, FERREIRA M S, BIERLICH J, et al. Hollow microsphere combined with optical harmonic Vernier effect for strain and temperature discrimination[J]. Optics & Laser Technology, 2020, 127: 106198.
[17] LIU Shuang, LU Guangwei, LV Dongyu, et al. Sensitivity enhanced temperature sensor with cascaded Sagnac loops based on harmonic Vernier effect[J]. Optical Fiber Technology, 2021, 66: 102654.
[18] WU Binqing, ZHAO Chunliu, XU Ben, et al. Optical fiber hydrogen sensor with single Sagnac interferometer loop based on Vernier effect[J]. Sensors and Actuators B: Chemical, 2018, 255: 3011-3016.
[19] WU Binqing, ZHAO Chunliu, XU Ben. Optical fiber temperature sensor with single Sagnac interference loop based on Vernier effect[C]. 2017 Conference on Lasers and Electro-Optics Pacific Rim (CLEO-PR), 2017: 1-3.
[20] LI Zeren, DANG Wenjie, DAN Jinxiao, et al. High-sensitivity interferometric high-temperature strain sensor based on optical harmonic Vernier effect[J]. Optical Fiber Technology, 2023, 79: 103361.

Fiber Optic Temperature Sensor Based on Harmonic Vernier Effect of Sagnac Interferometer

YANG Yuqiang[1,2,3], ZHANG Yuying[2,3], LI Yuting[2,3], GAO Jiale[2,3], MU Xiaoguang[4], BI Lei[5]
(1 *Shenzhen Institute, Guangdong Ocean University, Shenzhen* 518120, *China*)
(2 *Guangdong Provincial Key Laboratory of Intelligent Equipment for South China Sea Marine Ranching, Guangdong Ocean University, Zhanjiang* 524088, *China*)
(3 *Research Center of Guangdong Smart Oceans Sensor Networks and Equipment Engineering, Guangdong Ocean University, Zhanjiang* 524088, *China*)
(4 *College of Mechanical Engineering, Guangdong Ocean University, Zhanjiang* 524088, *China*)
(5 *College of Continuing Education, Guangdong Ocean University, Zhanjiang* 524088, *China*)

Abstract: Fiber optic interferometer has the advantages of small size, light weight, anti-corrosion, anti-electromagnetic interference, high sensitivity, etc., and is widely used in the measurement of temperature, humidity, magnetic field and other parameters. In recent years, researchers have dramatically improved the measurement sensitivity of interferometric fiber-optic sensors by cascading or paralleling two fiber-optic interferometers to produce an optical Vernier effect. When the free spectral ranges of the two fiber optic interferometers are close but not equal, the resulting Vernier effect is called the normal Vernier effect, when the free spectral range of one fiber optic interferometer is about an integer multiple of the other fiber optic interferometer, the resulting Vernier effect is called the harmonic Vernier effect.

In this paper, a parallel optical fiber temperature sensor based on two Sagnac interferometers is proposed, where the interferometers SI1 and SI2 are connected to the two outputs of the fiber-optic coupler C3, where SI1 is a reference interferometer and SI2 is a sensing interferometer. When the length of the Panda fiber in the SI2 interferometer is approximately $i+1$ of the length of the Panda fiber in the SI1 interferometer (i is 1, 2, 3 …) times, the two interferometers will produce an i-order harmonic Vernier effect. When i is 0, it produces an normal Vernier effect, at which time there will be a single envelope in the interference spectrum. When i is 1, it produces a first-order harmonic Vernier effect, at which time there will be a double envelope in the interference spectrum. When i is 2, it produces a second-order harmonic Vernier effect, at which time there will be a triple envelope in the interference spectrum. In other cases, the order is analogous. We have numerically simulated the theoretical analysis and the free spectral range of the interferometric spectrum of the length interferometer SI1 with a Panda fiber of 520 mm at constant temperature is 9.13 nm. The SI2 interferometers with lengths of 572 mm, 953 mm, and 1 430 mm of the Panda fiber have free spectral ranges of 8.30 nm, 4.98 nm, and 3.32 nm, respectively.

When the temperature is increased from T_0 ℃ to T_0+1 ℃, the interference spectra of SI2 interferometers with different Panda fiber lengths are all shifted to the short-wave direction, and the shifts are all about 1.89 nm, which is consistent with the theoretical analysis. The parallel interference spectra of interferometer SI1 and SI2 with Panda fiber lengths of 572 mm, 953 mm and 1 430 mm show single, double and triple envelopes respectively, indicating that the two interferometers produce the normal Vernier effect, first-order and second-order harmonic Vernier effects, respectively, and from the theoretical calculations. It can be seen that the amplification of the normal Vernier effect, first-order and second-order harmonic Vernier effects are all 11 times. When the temperature increases from T_0 ℃ to T_0+1 ℃, the single envelope moves in the short-wave direction, while the double and triple envelopes both move in the long-wave direction, which is opposite to that of the single SI2. In addition, the shifts of the single, double and triple envelopes are all about 20.7 nm due to the fact that the Vernier magnification is the same for the normal Vernier effect, first-order and second-order harmonic Vernier effects.

It is experimentally concluded that the interference spectra of SI2 are blueshifted in the temperature range from 40 ℃ to 50 ℃, and the shifts are all about 1.89 nm , which is consistent with the theoretical analysis and simulation results. The temperature sensitivity of the sensor corresponding to the normal Vernier effect is −20.67 nm/℃, the temperature sensitivity of the sensor corresponding to the first-order harmonic Vernier effect is 21.34 nm/℃, the temperature sensitivity of the sensor corresponding to the second-order harmonic Vernier effect is 21.18 nm/℃, and the fiber optic sensors corresponding to the harmonic Vernier effect and the normal Vernier effect have almost the same temperature sensitivities, which are both about 21 nm/℃. This results are consistent with the theoretical analysis and simulation results. The above experimental results show that the temperature sensitivity of the SI2 interferometer is independent of the length of the Panda fiber, although the magnification is the same, the harmonic Vernier effect and the normal Vernier effect correspond to the detuning of the length of the Panda fiber are obviously different, the detuning corresponding to the normal Vernier is 52 mm, and the detuning corresponding to the first-order and second-order harmonics is −87 mm and −130 mm, respectively. This shows that the higher the order, the larger the detuning amount, which is approximately a multiple increase. The above experimental results are consistent with the theoretical analysis. Since the larger the detuning amount, the easier the Vernier magnification can be controlled and realised, the harmonic Vernier effect is obviously superior to the normal Vernier effect from the preparation point of view. This study can provide an important reference for the subsequent study of optical Vernier effect.

Key words: Optical fiber sensor; Sagnac interferometer; Harmonic Vernier effect; Normal Vernier effect; Temperature sensing

OCIS Codes: 060.2370; 060.2310; 060.2300; 060.2430

Foundation item: Natural Science Foundation of Guangdong Province (Nos. 2023A1515011212, 2022A1515011603), Natural Science Foundation of Shenzhen City (Nos. JCYJ20210324122813036, JCYJ20220530162200001), Guangdong Provincial Ordinary Colleges and Universities Key Field Special Project (No. 2021ZDZX1015), Research Start-up Funding Project of Guangdong Ocean University (No. 060302112009)